Bending shape recovery of unidirectional carbon fiber reinforced epoxy-based shape memory polymer composites

Fengfeng Li [a, b], Fabrizio Scarpa [b, c], Xin Lan [d], Liwu Liu [a], Yanju Liu [a, *], and Jinsong Leng [d, *]

a. Department of Astronautical Science and Mechanics, Harbin Institute of Technology (HIT), P.O. Box 301, No. 92 West Dazhi Street, Harbin 150001, People's Republic of China

b. Bristol Composites Institute (ACCIS), University of Bristol, Bristol BS8 1TR, UK

c. Dynamics and Control Research Group (DCRG), CAME, University of Bristol, BS8 1TR, UK

d. Centre for Composite Materials, Science Park of Harbin Institute of Technology (HIT), P.O. Box 3011, No. 2 YiKuang Street, Harbin 150080, People's Republic of China

** corresponding author at: Department of Astronautical Science and Mechanics and Centre for Composite Materials of Harbin Institute of Technology, Harbin 150001, People's Republic of China, email addresses: yj_liu@hit.edu.cn (Y. Liu), lengjs@hit.edu.cn (J. Leng)*

Abstract: The thermo-mechanical properties of unidirectional carbon fiber reinforced epoxy-based shape memory polymer (SMP) composites with fiber mass fractions of 16%, 23%, 30%, 37% are evaluated by using three-point bending tests. The SMP composites show temperature-dependent flexural modulus and strength, with one order of magnitude difference between 120 °C and 20 °C. The composites show good shape recovery capability, with measured recovery ratios of more than 93% at 120 °C and 100% after 20 minutes at that temperature. The recovery stresses increase nonlinearly during reheating; the maximum recovery stress is approximately proportional to the fiber mass fraction. The composites show recovery capability under external loads, with the recovery ratio being inversely proportional to the partial load level. The composites feature good shape memory properties during cyclic loading and unloading at 120 °C. Their loss factors and stiffness losses decrease significantly during the first three cycles, and then stabilize after ten cycles.

Keywords: shape memory polymer composite, unidirectional carbon fiber, isothermal mechanical property, shape recovery property, three-point bending

1. Introduction

Shape memory polymers (SMP) have gained popularity as bases for high-performance composites. SMP composites are made using particles, fibers or fabrics as reinforcement, and shape memory polymer as the matrix [1-6].SMP composites can be easily manipulated into various configurations, and transfer from a deformed state to the original configuration under certain stimuli [2-5], mainly temperature [3, 5]. SMP composites start from an original shape (Figure 1), and are then deformed to a temporary shape by external forces at a temperature above the glass transition (Tg). After that, the SMP composites are cooled below Tg when subjected to external constraints, which. are removed once the SMP composites are fixed. Finally, the SMP are reheated above Tg and recover to their original shape. The mechanical and activation properties of SMP composites depend on their formulation. The carbon fiber or fabric reinforcement in SMP composites enhances the general mechanical performance of these laminates, and especially their shape recovery force [4, 5, 7]. SMP composites also feature low density, adjustable Tg and high damping capability, which make these active composites suitable for aerospace applications, such as hinges, trusses, antennas, and solar arrays [2-13].

Existing open literature shows many examples of the design, fabrication and tests of structures made of SMP composites. Only a minority of published papers deals with experiments to fully characterize fiber or fabric reinforced SMP composites. These latter papers could be broadly divided into two categories: one related to unidirectional fiber reinforced SMP composites and their microstructural mechanisms occurring during bending [7, 8, 10, 14-18]. The other group of papers concerns the analysis of the thermo-mechanical behavior of fabric reinforced SMP composites [11-13, 19-27]. Since 1999, Composite Technology Development, Inc. has been developing SMPs and related fiber reinforced composites (Elastic Memory Composite, EMC) [7, 8, 14, 15, 20]. Papers generated by teams of researchers associated to the company have focused on the out-of-plane and in-plane buckling of unidirectional carbon fiber reinforced EMCs [14, 15]. One of the main conclusions of these works is the presence of micro-buckling of the fibers, because the soft matrix does not possess sufficient stiffness to support the fiber under compression [14, 15]. Micro-buckling however allows the whole composite to undergo large bending deformations. Lan et al. and Zhang et al. have further explored the phenomenon of micro-buckling, with a series of experimental and analytical studies related to the influence of the neutral plane, critical buckling, fiber buckling half-wavelength and amplitude of unidirectional carbon fibers in reinforced SMP composites [16, 17].

As stated above, the thermo-mechanical behavior of SMP composites is an object of interest for several research teams [18-26]. Early works have focused on the evaluation of prototypes making use of the SMP effect, like furlable truss boom [7], EMC hinge [8], and reflector [20]. In those studies emphasis was placed on the packaging and other factors like deployment torque, precision, and repeatability. Those works have been of value to assess the feasibility of above prototypes, but have not provided a comprehensive constitutive modelling of the materials, in particular to describe the shape recovery properties [18-22]. Some works merely describe combinations of SMP constitutive models with composite laminate theory and related finite element representations (see Tan et al. [23], Roh et al. [24], Gu et al. [25]).

There is however a notable lack of experimental data to characterize in a meaningful and exhaustive way the theoretical studies around SMP composites. In 2012, Fejős et al. have performed constrained and unconstrained recovery tests of composite made from woven glass fabric reinforced epoxy-based SMP with a fiber mass fraction of 38%. The tests were performed using three-point bending loading in a dynamic mechanical analysis (DMA) device. In that study the researchers found that the shape fixity would be decreased because of the reinforcement, while the shape recovery stress improved [26]. The following year Fejős quantified the shape memory characteristics of carbon fabric asymmetrically reinforced SMP composite by using the same testing technique [27]. In these two studies, the maximum strains within the experiments were between 1% and 2.5%. The maximum level of strains and forces in a DMA (typical around 18 N) are however inadequate to allow carbon fiber or fabric reinforced SMP composites to undergo large deformations, and therefore exploit the potential of these smart composites within their full design space, in particular for what it concerns the shape recovery behavior.

The novelty of the work described in this paper is about the focus on a series of three-point bending experiments related to unidirectional carbon fiber reinforced SMP composites with fiber mass fractions of 16%, 23%, 30% and 37%. The epoxy-based SMP inherits the properties of the conventional epoxy resins, while at the same time possessing shape memory properties [28, 29]. The matrix of this composite is less expensive to manufacture than other SMPs, such as cyanate-based [30, 31]. Carbon fiber has been chosen as the reinforcement mainly because of its high specific stiffness and strength, and robust chemical and thermal stability [32]. Although Kevlar and PBO fibers possess higher mechanical properties, their relatively high cost make them less suitable for large-scale productions, although they could be considered for other high-end applications [33]. Bending tests are chosen because they are representative of the real main deformation occurring in the operation of these composites. In particular, isothermal bending stress-strain experiments are performed to obtain values of the yield stress and strength at failure break strength at different temperatures. Free recovery experiments are also conducted to assess the shape recovery; other experiments carried out here are the constrained displacement recovery to evaluate the stress response for increasing temperatures, and partial load recovery during reheating, and the cyclic loading at 120 ^{o}C to assess the residual deformation of the SMP composites. The main contribution and novelty of this work is different from previous works by others, providing a series of three-point bending experiments of unidirectional carbon fiber reinforced SMP composites with various fiber mass fractions. These studies not only allow a mechanical characterization of the manufactured SMP carbon reinforced materials for direct engineering applications, but also provide reference value of the composite that could then be used to design and optimize new generations of SMP unidirectional reinforced materials by adjusting the type of the fiber, mass fraction and stacking sequences architectures.

2. Material preparation

The matrix used in this study is an epoxy-based SMP, which has been subjected to ground-simulated space environment tests [28]. The Tg of the matrix is 89.3 ^{o}C (Figure 2), conducted by a dynamic mechanical analysis (DMA) test by a DMA 242 C analyfzer (NETZSCH Instruments, Germany) with tension mode over a temperature range from 30 ^{o}C to 160 ^{o}C at a heating rate of 3 ^{o}C/min and a frequency of 1 Hz. And the reinforcement is carbon fiber T700SC-12K (TORAY), the carbon fiber properties can be

found in reference [34]. Four types of carbon fiber reinforced SMP composites have been fabricated, with fiber mass fractions of 16%, 23%, 30% and 37%, respectively. To obtain a fixed and controllable thickness (2mm in this study) and a uniform fiber distribution in the composite sheet, we have modified the conventional unidirectional fiber reinforced composite fabrication (Figure 3). Here we have added some seal strips made of die steel at the bottom, left, and right sides of the curing plate mold, and control the thickness of filler strip between every layer. The rotating mandrel has also been divided into three parts: a rectangle plate for the winding filament, and two handles to connect the rectangle plate and the spindle.

A filament winding machine is used to produce the dry unidirectional carbon fibers (no resin) at variable layers of 2, 3, 4, and 5, which corresponding to fiber mass fraction of 16%, 23%, 30% and 37%. After finishing one layer the machine was paused, and stuck calculated thickness filler strip at edges, vertical to fiber orientation, before continuing the winding. The dry carbon fibers rectangular plate assembly was then placed in the middle of curing plates. The surfaces were then sealed and the SMP epoxy-based resin was poured into the assembled curing mold. The curing was performed at 80 ^{o}C for 3 hours, followed by 100 ^{o}C for 3 hours and 150 ^{o}C for 5 hours. The composite sheets were then de-moulded and cut into the required dimensions by CNC engraving and milling. Since the SMP composites here were categorized as laminated thermosetting materials and the three-point bending ASTM D790-17 test was performed, all specimens were cut into dimension of 2 mm in thickness, 12.7 mm in width and 60 mm in length [35].

3. Thermo-mechanical experiments

All experiments presented in this study are performed using a Zwick Z010 universal testing machine with a three-point bending rig. The machine is equipped with a 1 kN load cell (Zwick GmbH, Ulm, Germany). The indenter and the two support rollers all have cylindrical surfaces with diameters of 10.0 mm. The support span is 32 mm, with a span-to-depth ratio of 16:1. A temperature chamber (Zwick GmbH, Ulm, Germany) with range of -80 ^{o}C to +250 ^{o}C has been used; its liquid nitrogen cooling system has the capability of maintaining the required temperature within $\pm$ 3 ^{o}C of the nominal temperature. All five types of experiments have a target high temperature of 120 ^{o}C. The three recovery experiments (free, constrained displacement and partial load) underwent a programmed temperature change. All specimens used in this work were unidirectional in terms of alignment of the fibers (i.e., the fibers are at 0^{o}).

The isothermal bending tests were carried out first by heating the specimens to target temperatures (20 ^{o}C, 40 ^{o}C, 60 ^{o}C, 80 ^{o}C, 100 ^{o}C, 120 ^{o}C) at a heating rate of 3 ^{o}C/min. The specimens were then left at the target temperature for at least 20 minutes. Two thermocouples have been attached at specimen middle front and back surfaces to monitor the state of the temperature. The specimens were preloaded at 2 N with a crosshead velocity of 1 mm/min. The bending tests were then carried out at 0.8 mm/min and were terminated when either the strain reached 0.05 mm/mm, or the specimen broke before reaching the 0.05 mm/mm.

During the free recovery experiments the specimens would experience a programmed temperature change from 30 ^{o}C to 120 ^{o}C. In this experiment, only the fiber mass fraction is varied amongst the specimens; the other test parameters (heating or cooling rate, maximum deflection and loading rate) were

kept constant. The dimensions of the specimens and the experimental setup were similar to the ones of the isothermal bending tests. A complete free recovery cycle consists of, heating, followed by the deformation, cooling, re-adjustment of the loading lever and final reheating. In this work we have performed two continued free recovery cycles to evaluate the repeatability of the experiment. The specimens were placed in the middle of the two supports, with a 2 mm gap between the indenter and the specimen. The specimens were then preloaded at 2 N with crosshead rate of 1 mm/min, and heated to 120 ^{o}C at a heating rate of 3 ^{o}C/min. Once the 120 ^{o}C were reached the specimens were kept at that temperature for 20 minutes to allow the system to reach its thermal equilibrium. The specimens were then deformed to a maximum deflection of 4 mm with a crosshead rate of 0.8 mm/min. At that position the specimens were cooled to reach 30 ^{o}C at 3 ^{o}C/min, and then left at that temperature for 20 minutes. After that interval of time the loading was adjusted in load control to 0.1 N with a crosshead velocity 1 mm/min. The very low preload gives the specimen a virtual free load state, but still allows the measurement of the deflection at the contact between indenter and SMP composite. In that position the specimens were reheated to 120 ^{o}C at 3 ^{o}C/min, and left for 20 minutes. All these steps were repeated twice.

The constrained displacement recovery was also carried out in two repeated cycles. In this case the first five steps of the procedure were the same of the free recovery described before. The indenter was then adjusted to reach a 0.1 N preload under load control, and with the indenter in that position the specimens were first reheated to 120 ^{o}C at a heating rate of 3 ^{o}C/min, and kept at that temperature for 20 minutes before starting the next sub-cycle (cooling/reheating).

The partial load recovery experiments aimed at studying the effect of a partial load on the recoverability of the SMP composites. Only two types of materials have been tested (fiber mass fractions of 23% and 37%). The partial loads applied were 25%, 50% and 75% of the maximum recovery force obtained from the constrained displacement recovery experiments. The steps were similar to the free recovery experiments (preload of 2 N at 30 ^{o}C, heating to 120 ^{o}C, 20 minutes of stabilization, maximum deflection under displacement control, cooling to 30 ^{o}C, stabilization at that temperature). Under load control, loads of 6.5 N, 13.0 N, 19.5 N on specimens with fiber mass fraction of 23% have been applied. The specimens with 37% of mass fraction were subjected to loads of 12.5 N, 25 N and 37.5 N. Those loads were held while the specimens were re-heated to 120 ^{o}C at 3 ^{o}C/min.

Further cyclic loading and unloading experiments were conducted at a temperature of 120 ^{o}C to assess the repeatability of the deformation at high temperature. The procedure in those tests was similar to the one used before (preload of 2 N at 30 ^{o}C, heating to 120 ^{o}C and 20 minutes of stabilization). The specimens were then subjected under load control to a 0.1 N preload at 1 mm/min, followed by displacement control loading at maximum deflection for 14 cycles.

4. Results and discussion

The SMP composites with different fiber mass fractions show a stiffening response at 20 ^{o}C (Figure 4 (a)-(d)) under isothermal bending. At that temperature the specimens exhibit the presence of a crack across the outer surface under the indenter that does not penetrate across the thickness. The specimens yield with the increase of the temperature, and fail at 40 ^{o}C and 60 ^{o}C with the exception of the 16 wt.% that break before yielding. At above 80 ^{o}C the specimens yield before the 4.26 mm deflection. The

maximum stresses at 100 °C and 120 °C are about one order of magnitude lower than that the one at 20 °C for same type of SMP composite.

The flexural stress σ_f and modulus E_f of the SMP composites can be calculated as [25]:

$$\sigma_f = \frac{3FL}{2bd^3} \tag{1}$$

$$\varepsilon_f = \frac{6Dd}{L^2} \tag{2}$$

$$E_f = \frac{mL^3}{4bd^3} \tag{3}$$

In (1)-(3) F is the load, L is the support span, b is the width and d is the depth of specimen, D is the predetermine maximum deflection of the center of the specimen, and m is the slope of the tangent to the initial straight line of the load-deflection curve.

Figure 5 shows the flexural modulus and strength of the composites. Every curve shows a clear turning point around 80 °C, since that temperature is close to the Tg of 89.3 °C, and the matrix gradually changes from glassy to rubbery state. The flexural modulus and the strength increase with the increasing fiber mass fractions at the same temperature. The rate of increase varies however with the temperature. For example, the rates of increase of the flexural modulus at 60 °C are 280% (37 wt.%), 250% (30 wt.%), and 130% (23 wt.%) higher than the value of 16 wt.%. These rates are however significantly higher at 20 °C, and are 400% (37 wt.%), 300% (30 wt.%), 200% (23 wt.%) higher than the value of the 16 wt.% specimens. This is expected, since at low temperature the bonding between matrix and fiber is high and the reinforcement effect of the fiber increases almost linearly with the increase of fiber content. At high temperatures the matrix softens, the bonding strength decreases, with a resulting fiber reinforcement effect showing a nonlinear decline.

The results of the free recovery experiments are shown in Figure 6. The flexural stress and strain are calculated by equations (1) and (2). The flexural stress is initially constant, while the flexural strain slightly decreases due to the thermal expansion of the specimen along its depth. The flexural stress and strain then increase linearly during deformation process. During cooling the strain maintains the last value of the previous test phase and the stress decreases nonlinearly from ~ -7 MPa to ~ -2 MPa. The stress is however supposed to be 0 MPa, the reason for the negative values is the thermal contraction of the specimen which causes a small gap of ~ 0.3 mm between the indenter and the specimen. The air flow caused by the fan in the chamber goes through the gap and creates a dynamic pressure felt by the load cell. Before reheating the indenter must automatically adjust to the position corresponding to 0.1 N, therefore a step between strain and stress appears at the end of cooling process. We can consider the position after the step as the starting one to evaluate the recovery of the SMP composites in the following results. During the first reheating phase the 0.1 N load is maintained on the specimen, and this allows the specimen some freedom to recover. A significant decrease of the strain is observed close to the Tg as a result of the matrix transitioning to the rubber phase rapidly. The temperature and strain curves have a good repeatability across the two cycles, and the additional strains of the indenter (i.e., the one produced by the step due to the negative force) before the two reheating processes are almost the same. The maximum stress during

the two deformation processes and the additional strain before the two reheating phases are presented in Table 1. The maximum stress during the second deformation process has 9%-30% decrease compared to the first cycle and varies with the fiber mass fraction. The decline might be caused by internal microcracks in the specimens generated during the manufacturing stage and deformation process. No visible damage, such as delamination or fiber fracture, has been however observed.

To evaluate the recoverability of the SMP composites, the experimental results during the first reheating process are used to formulate a recovery ratio [36]:

$$R = \frac{l - x}{l} \tag{4}$$

In (4) R is the recovery ratio, l is the deflection at the beginning of the reheating process and x is the deflection during the reheating process. Figure 7 presents the recovery ratio as a function of the temperature for the four types of SMP composites after the first recovery cycle. The recovery ratio below 60 ^{o}C is nearly zero, since the temperature is far below the Tg and no phase transition in the matrix occurs. When the temperature goes over the Tg the matrix phase transitions gradually to rubber, thus the recovery ratio increases and reaches its peak. The recovery ratio then decreases as the storage strain of the specimen is released. The final recovery ratios are 96%, 95%, 93%, and 94% for the materials with fiber mass fractions of 16%, 23%, 30% and 37%, respectively. Since the data shown here are related to the temperature just reaching 120 ^{o}C, the recovery ratios calculated after holding the specimens for other 20 minutes reach nearly 100%.

The constrained displacement recovery tests also have two continued recovery cycles starting from the temperature reaching 120 ^{o}C. The temperature, flexural strain and stress curves during the first deformation and cooling are almost the same as in free recovery experiments (Figure 8). The step responses between strain and stress are also present. During the first reheating process the strain remains constant and the stress arises nonlinearly. The maximum stress is presented within the 20 minutes stabilization at 120 ^{o}C. The stress then gradually decreases during the following cooling and reaches a negative value, as in the free recovery experiment. Another additional strain is presented during the second cooling process. The shape of the stress curve during the second reheating is similar to the one during the first reheating process. The recovery stress is the reaction stress of the specimen to the indenter. The maximum recovery stresses during the two reheating processes are presented in Table 2, along with the additional strains before reheating. The maximum recovery stress during the second cycle is ~ 4%-12% lower compared to the one of the first cycle, and this might be the presence of internal damages in the specimen during the deformation. The additional deflections before reheating are almost the same in the two cycles.

The recovery stress versus the temperature for various mass fractionsis shown in Figure 9. The negative stress has been here ignored, since it is caused by the aforementioned dynamic pressure. The slope of the four curves within 30 ^{o}C-70 ^{o}C increases with the increase of the fiber mass fraction, and this is also due to the excellent thermal conductivity and stiffness of the carbon fiber compared to the epoxy resin. An evident bulge can be observed for SMP composites with fiber mass fractions of 23%, 30% and 37%. Furthermore, one can observe a bulge appearing during reheating, which then disappears during

cooling (see the details for a fiber mass fraction of 37% in Figure 10). Since during reheating the internal heat within the material builds up with the increase of temperature, the accumulated heat at ~ 80 °C can trigger the rapid release of the stored strain energy of the SMP composite. At high temperatures (100 °C-120 °C) the recovery stress changes slowly and maintains a relatively high value. The maximum recovery stress of the SMP composite with 16% of fiber mass fraction is 16.5 MPa, and 24.3 MPa, 39.6 MPa, and 49.0 MPa for fiber mass fractions of 23 %, 30 % and 37 %, respectively. The increase ratios are 47.7% (23 wt.%), 140.3% (30 wt.%), and 197.5% (37 wt.%) corresponding to that of for 16 wt.%, almost a linear increase among the fiber mass fraction.

The results of the partial load and free recovery experiments (the latter only related to the first reheating cycle) are shown in Figure 11. The recovery force within the same type of SMP composite varies from specimen to specimen, due to tolerance mismatch and experimental errors. The partial load here is calculated as the average of the recovery force in the constrained displacement recovery. During reheating the specimen is loaded elastically at first, leading to an increase of the flexural strain with the partial load increase at 30 °C. The additional strain at the beginning of the reheating process is still mainly caused by the thermal contraction during cooling. The evident shape recovery for all the SMP composites used in this work begins at ~ 80 °C, however the range of temperatures corresponding to the fastest recovery rate varies from composite to composite (85 °C-100 °C for 0% F, 95 °C-105 °C for 25% F, 100 °C-120 °C for 50% F and 75% F). This is a logical consequence of the results shown in Figure 9: the recovery stress increases with the temperature, therefore the specimens need to reach the temperature that could trigger a sufficient recovery stress to overcome the applied partial load.

The recovery ratios have been calculated by using equation (4), where l is the deflection value at the beginning of reheating process, however in this case x is the deflection when the temperature just reaches 120 °C. The values at constant percentage of maximum recovery force are approximately identical for the two composites at 23% and 37% of carbon fiber mass fraction (Figure 12). The average recovery ratios when the temperature just reaches 120 °C are 94%, 71%, 37%, and 9% of the total deflection at the beginning of reheating, under partial loads accounting for 0%, 25%, 50% and 75% of the maximum recovery force, respectively. The specimens subjected to low partial load are capable of larger recovery ratio compared to those under high partial loads.

Figure 13 (a)-(d) show the flexural stress-strain relationships of the cyclic loading and unloading experiments with different fiber mass fractions at 120 °C. At that temperature the matrix behaves as an hyperelastic material in rubber phase. Most applications involving SMP composites require specific levels of deformation, so here we are concerned about the repeatability of the material subjected to the same maximum deformation rather than load. An obvious hysteresis is present, and that reflects the energy dissipation caused by the internal friction within the material. The maximum stiffness and the integral value of the hysteresis loop gradually decreases with the increase of the number of cycles. Here use the method of the static hysteresis loop of the stress-strain curve of the specimen under the cyclic loading to characterize the energy dissipation. The loss factor is proportional to the ratio of energy loss, ΔW in a vibration cycle to the amplitude value of the potential energy in a cycle, W, it is depend upon the parameters of the manipulator and control system [37]. Due to the shape of the hysteresis loop, We define

here the loss factor as:

$$\eta = \frac{\Delta W}{2\pi W} \tag{5}$$

Where η is the loss factor, ΔW is the energy loss equal to the area of the hysteresis loop, and W is the potential energy equals to the area underneath by the stress/strain curve during cooling. The stiffness loss can be expressed as σ/σ_0, where σ is the maximum stress during at cycle and σ_0 is the one corresponding to the first cycle.

The loss factor and stiffness loss at every cycle are shown in Figures 14 (a) and (b). In all types of SMP composites, the first cycle loss factor is the largest, while the second or third cycles correspond to the lowest, and that value gradually increasing with increments lower than 1% compared to the lowest attained. The 16 wt.% loss factor curve is above the 23 wt.%, and the loss factor values of the 30 wt.% SMP composites are always lower than the 23 wt. %. The 37 wt.% curve is sandwiched between the 16 wt.% and the 23 wt.% curves, which indicates that the loss factor at every cycle follows a concave curve with the increase of the fiber mass fraction. The stiffness loss decreases rapidly during the first three cycles, with the decrease rate attenuating after fifth cycle, and almost nearly stabilizing after tenth cycle. For every cycle the SMP composites listed by carbon fiber mass fraction in order to increasing stiffness losses are the 16 wt.%, 37 wt.%, 23 wt.% and 30 wt.%. After 15 cycles the stiffness losses range between ~ 67% and ~ 85%.

The reason for the decline of the loss factor and stiffness loss during the first cycles could be attributed to the relatively high shear stress between fiber and matrix inside the specimen causes internal microcrak initiation, which can be referred to Figure 8 in reference [16]. Although the optical microscopic images of microstructure of SMPC specimen in reference [16] is after 50 bending cycles, considering the damage is a accumulated process and the significant decline of loss factor and stiffness loss in Figure 14 of this study, we have reason to believe there is microcrack initiation after first cycle. The loss factor increases slightly after the third cycle since the internal friction (stick-slip effect) between matrix and fibers dissipates energy. The microcrack growth however attenuates with the increase of cycles, thus the stiffness loss decreases slightly and nearly stabilizes after the tenth cycle. Since the stiffness loss changes sharply before the third or fourth cycle, and trends to stabilize in the subsequent cycles, thus we call the first three or four cycles as training process. In practical applications, if we want to have a relatively stable stiffness, we could first train the SMP composite components three or four times before they can be put into use. It should be realized that the matrix is at its rubbery phase and has higher damping ratio than that at room temperature since this kind of experiment is carried out at 120 ^{o}C. Because the SMP composite with the carbon fiber mass fraction of 16% has more matrix proportion, it dissipates more energy than others, resulting in the highest ranking of the loss factor and the biggest stiffness loss compared to others. For those SMP composites with low fiber mass fraction, the damping ratio decreases with the increase of fiber mass fraction. As the fiber mass fraction increases, the microcracks dominate the damping capacity and dissipate more energy. Therefore the loss factor and stiffness loss of SMP composite with fiber mass fraction 37% decreases, sandwiched between the 16 wt.% and the 23 wt.%.

5. Conclusions

Experiments have been performed on unidirectional carbon fiber reinforced SMP materials with four levels of fiber mass fractions to evaluate the thermo-mechanical properties of these composites by three-point bending. The flexural modulus and strength show clear turning points around 80 ^{o}C since the matrix massively transfers from the glassy to rubbery state, their values at the temperatures 100 ^{o}C and 120 ^{o}C are about one order of magnitude lower than that the one at 20 ^{o}C for same type of SMP composite. Their values increase with the increasing fiber mass fractions at the same temperature, but the increase rate shows a nonlinear decline with the temperature increase. The free recovery experiment shows that the SMP composites recover rapidly transitioning through Tg since the matrix largely transfers from the glassy to rubbery state; the recovery ratios are 96% (16 wt.%), 95% (23 wt.%), 93% (30 wt.%), and 94% (37 wt.%) at 120 ^{o}C, and 100% after 20 minutes at 120 ^{o}C. The results repeat well in second cycle. In the constrained displacement recovery experiment the recovery stress increases nonlinearly during reheating; for a constant temperature, the larger the fiber mass fraction, the higher the recovery stress; the maximum recovery stresses for different SMP composites are 16.5 MPa (16 wt. %), and 24.3 MPa (23 wt. %), 39.6 MPa (30 wt. %), and 49.0 MPa (37 wt. %) at the first cycle, while ~ 4%-12% lower at the second cycle. The SMP composites still have the capability to recover to a certain configuration under an external load, as long as the latter is smaller than the maximum recovery force. The recovery ratios for SMP composite with different fiber mass fraction are approximately identical at the same partial load level, and inversely proportional to the partial load divided by the maximum recovery force. Finally, the results of the cyclic loading and unloading experiments at 120 ^{o}C demonstrate that the SMP composites can be deformed and recovered repeatedly without losing their shape memory property, though the maximum stress decreases after the first three cycles and then nearly stabilizes after 10 cycles. The loss factor also follows a similar trend, although with a more remarkable stabilization.

The contribution of this study is to systematically offer experimental data for unidirectional carbon fiber reinforced SMP composites. Not only does this study expand the know-how on the SMP composites free, constrained displacement and partial load recovery responses data available in open literature, but also addresses the the evaluation of the impact of the fiber mass fractions on the thermo-mechanical properties of shape memory polymer materials. The optimal mass fraction depends on the actual application conditions. For those who need large recovery stress but only once or twice deployment, the SMP composite with fiber mass fraction of 37% is recommended, since its recovery stress is the highest, and its loss factor and stiffness loss at the first two cycles are almost the same as others. For those who need a stable recovery behavior, we first recommend the SMP composite with lower fiber mass fraction, as long as it meets the recovery stress requirement.

Acknowledgments

This work is supported by the National Natural Science Foundation of China (Grant Nos: 11672086, 11772109 and 11632005) and China Scholarship Council.

Reference

[1] Tobushi H, Hara H, Yamada E, Hayashi S. Thermomechanical properties in a thin film of shape

memory polymer of polyurethane series. Smart Mater Struct 1996;5(4):483.

[2] Ratna D, Karger-Kocsis J. Recent advances in shape memory polymers and composites: a review. J Mater Sci 2008;43(1):254-69.

[3] Leng J, Lan X, Liu Y, Du S. Shape-memory polymers and their composites: stimulus methods and applications. Prog Mater Sci 2011;56(7):1077-135.

[4] Liu Y, Du H, Liu L, Leng J. Shape memory polymers and their composites in aerospace applications: a review. Smart Mater Struct 2014;23(2):023001.

[5] Mu T, Liu L, Lan X, Liu Y, Leng J. Shape memory polymers for composites. Compos Sci Technol 2018;160:169-198.

[6] Chen H, Xia H, Qiu Y, Ni Q. Analyzing effects of interfaces on recovery rates of shape memory composites from the perspective of molecular motions. Compos Sci Technol 2018;163:105-115.

[7] Keller P, Lake M, Francis W, Harvey J, Ruhl E, Winter J, et al. Development of a deployable boom for microsatellites using elastic memory composite material. 45th AIAA/ASME/ASCE/AHS/ASC Structures, Structural Dynamics & Materials Conference; 2004. p. 1603.

[8] Barrett R, Francis W, Abrahamson E, Lake M, Scherbarth M. Qualification of elastic memory composite hinges for spaceflight applications. 47th AIAA/ASME/ASCE/AHS/ASC Structures, Structural Dynamics, and Materials Conference 14th AIAA/ASME/AHS Adaptive Structures Conference 7th; 2006. p. 2039.

[9] Sokolowski WM, Tan SC. Advanced self-deployable structures for space applications. J Spacecr Rockets 2007;44(4):750-4.

[10] Rossiter J, Takashima K, Scarpa F, Walters P, Mukai T. Shape memory polymer hexachiral auxetic structures with tunable stiffness. Smart Mater Struct 2014;23(4):045007.

[11] Li F, Liu L, Lan X, Wang T, Li X, Chen F, et al. Modal Analyses of Deployable Truss Structures Based on Shape Memory Polymer Composites. Int J Appl Mechanics 2016;8(07):1640009.

[12] Liu T, Liu L, Yu M, Li Q, Zeng C, Lan X, Liu Y, Leng J. Integrative hinge based on shape memory polymer composites: Material, design, properties and application. Compos Struct 2018;206:164-176.

[13] Dao TD, Ha NS, Goo NS, Yu W-R. Design, fabrication, and bending test of shape memory polymer composite hinges for space deployable structures. J Intell Mater Syst Struct 2018;29(8):1560-74.

[14] Francis W, Lake M, Mayes JS. A review of classical fiber microbuckling analytical solutions for use with elastic memory composites. 47th AIAA/ASME/ASCE/AHS/ASC Structures, Structural Dynamics, and Materials Conference 14th AIAA/ASME/AHS Adaptive Structures Conference 7th; 2006. p. 1764.

[15] Francis W, Lake M, Schultz M, Campbell D, Dunn M, Qi HJ. Elastic memory composite microbuckling mechanics: closed-form model with empirical correlation. 48th AIAA/ASME/ASCE/AHS/ASC Structures, Structural Dynamics, and Materials Conference; 2007. p. 2164.

[16] Lan X, Liu L, Liu Y, Leng J, Du S. Post microbuckling mechanics of fibre-reinforced shape-memory polymers undergoing flexure deformation. Mech Mater 2014;72:46-60.

[17] Zhang J, Dui G, Liang X. Revisiting the micro-buckling of carbon fibers in elastic memory

composite plates under pure bending. Int J Mech Sci 2018;136:339-48.

[18] Lan X, Liu Y, Lv H, Wang X, Leng J, Du S. Fiber reinforced shape-memory polymer composite and its application in a deployable hinge. Smart Mater Struct 2009;18(2):024002.

[19] Yee J, Soykasap O, Pellegrino S. Carbon fibre reinforced plastic tape springs. 45th AIAA/ASME/ASCE/AHS/ASC Structures, Structural Dynamics & Materials Conference; 2004. p. 1819.

[20] Keller P, Lake M, Codell D, Barrett R, Taylor R, Schultz M. Development of elastic memory composite stiffeners for a flexible precision reflector. 47th AIAA/ASME/ASCE/AHS/ASC Structures, Structural Dynamics, and Materials Conference 14th AIAA/ASME/AHS Adaptive Structures Conference 7th; 2006. p. 2179.

[21] Nji J, Li G. A self-healing 3D woven fabric reinforced shape memory polymer composite for impact mitigation. Smart Mater Struct 2010;19(3):035007.

[22] Ahmad M, Singh D, Fu YQ, Miraftab M, Luo J. Stability and deterioration of a shape memory polymer fabric composite under thermomechanical stress. Polym Degrad Stab 2011;96(8):1470-7.

[23] Tan Q, Liu L, Liu Y, Leng J. Thermal mechanical constitutive model of fiber reinforced shape memory polymer composite: based on bridging model. Compos Part A Appl Sci Manuf 2014;64:132-8.

[24] Roh J-H, Kim H-I, Lee S-Y. Viscoelastic effect on unfolding behaviors of shape memory composite booms. Compos Struct 2015;133:235-45.

[25] Gu J, Xie Z, Wang S, Sun H, Zhang X. Thermo-mechanical modeling of woven fabric reinforced shape memory polymer composites. Mech Adv Mater Struct 2018:1-11.

[26] Fejős M, Romhány G, Karger-Kocsis J. Shape memory characteristics of woven glass fibre fabric reinforced epoxy composite in flexure. J Reinf Plast Compos 2012;31(22):1532-7.

[27] Fejős M. Shape memory performance of asymmetrically reinforced epoxy/carbon fibre fabric composites in flexure. Express Polym Lett 2013;7(6):528-34.

[28] Leng J, Wu X, Liu Y. Effect of a linear monomer on the thermomechanical properties of epoxy shape-memory polymer. Smart Mater Struct 2009;18(9):095031.

[29] Yang X, Guo Y, Luo X, Zheng N, Ma T, Tan J, Li C, Zhang Q, Gu J. Self-healing, recoverable epoxy elastomers and their composites with desirable thermal conductivities by incorporating BN fillers via in-situ polymerization. Compos Sci Technol 2018;164:59-64.

[30] Xie F, Huang L, Liu Y, Leng J. Synthesis and characterization of high temperature cyanate-based shape memory polymers with functional polybutadiene/acrylonitrile. Polymer 2014;55(23):5873-5879.

[31] Gu J, Xu S, Zhuang Q, Tang Y, Kong J. Hyperbranched polyborosilazane and boron nitride modified cyanate ester composite with low dielectric loss and desirable thermal conductivity. IEEE Trans Dielectr Electr Insul 2017;24(2):784-790.

[32] Zhang Y, Tao W, Zhang Y, Tang L, Gu J, Jiang Z. Continuous carbon fiber/crosslinkable poly (ether ether ketone) laminated composites with outstanding mechanical properties, robust solvent

resistance and excellent thermal stability. Compos Sci Technol 2018;165:148-153.

[33] Tang Y, Dong W, Tang L, Zhang Y, Kong J, Gu J. Fabrication and investigations on the polydopamine/KH-560 functionalized PBO fibers/cyanate ester wave-transparent composites. Compos Commun 2018;8:36-41.

[34] TORAYCA® yarn Product data. <www.torayca.com/en/lineup/product/pro_001_01.html>.

[35] ASTM I. Standard test methods for flexural properties of unreinforced and reinforced plastics and electrical insulating materials. ASTM D790-072007.

[36] Tobushi H, Hayashi S, Hoshio K, Makino Y, Miwa N. Bending actuation characteristics of shape memory composite with SMA and SMP. J Intell Mater Syst Struct 2006;17(12):1075-1081.

[37] Zinoviev P A, Ermakov Y N. Energy dissipation in composite materials. CRC Press, 1994.

Figure Captions

Fig. 1. Shape memory cycle in three-point bending deformation mode.

Fig. 2. DMA result of epoxy-based SMP.

Fig. 3. Diagrams of the things required for material preparation, (a) mold, (b) arrangement of filler strip and fiber layer, (c) filament-winding.

Fig. 4. Flexural stress versus strain curves at different temperatures of unidirectional carbon fiber reinforced SMP composites, (a) 16 wt.%, (b) 23 wt.%, (c) 30 wt.%, (d) 37 wt.%.

Fig. 5. Mechanical properties at different temperatures for the unidirectional carbon fiber reinforced SMP composites at different fiber mass fractions (a) flexural modulus, (b) flexural strength.

Fig. 6. Free recovery experiment curves of unidirectional carbon fiber reinforced SMP composites, (a) 16 wt.%, (b) 23 wt.%, (c) 30 wt.%, (d) 37 wt.%, (e) images at different steps.

Fig. 7. Free recovery ratio-temperature curves of four types of SMP composites in the first free recovery cycle.

Fig. 8. Constrained displacement recovery experiment curves of unidirectional carbon fiber reinforced SMP composites, (a) 16 wt.%, (b) 23 wt.%, (c) 30 wt.%, (d) 37 wt.%, (e) images at different steps.

Fig. 9. Recovery stress-temperature curves of four types of SMP composites in the first constrained displacement recovery cycle.

Fig. 10. Flexural stress-temperature curves for UD carbon fiber reinforced SMP composite with fiber mass fraction of 37% (the red arrow indicates reheating, the blue arrow is for cooling).

Fig. 11. Flexural strain-temperature curves during partial load recovery for the SMP composites with fiber mass fraction of (a) 23 %, (b) 37 %.

Fig. 12. Recovery ratio of SMP composites with fiber mass fraction 23% and 37% under different partial load.

Fig. 13. Flexural stress versus strain curves of cyclic loading and unloading experiment of SMP composites with fiber mass fraction of (a) 16 %, (b) 23 %, (c) 30 %, (d) 37 % (the blue arrow indicates loading direction, the red arrow is for unloading direction, the black arrow represents the movement of the maximum load from cycle No. 1 to No. 15).

Fig. 14. Statistic of unidirectional carbon fiber reinforced SMP composites, (a) loss factor, (b) stiffness loss.

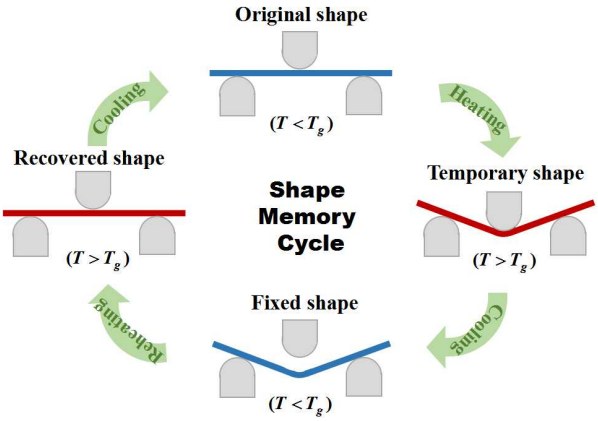

Fig. 1. Shape memory cycle in three-point bending deformation mode.

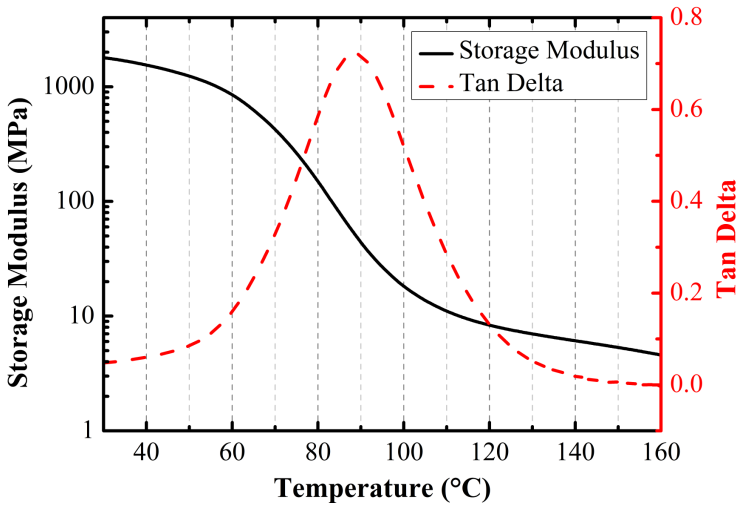

Fig. 2. DMA result of epoxy-based SMP.

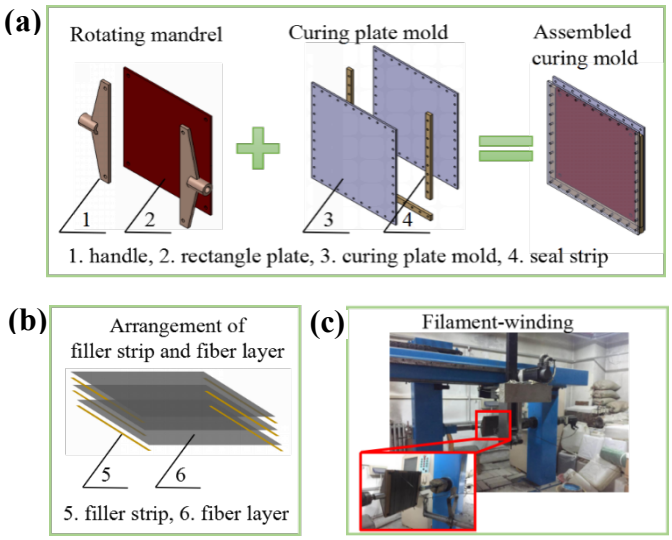

Fig. 3. Diagrams of the things required for material preparation, (a) mold, (b) arrangement of filler strip and fiber layer, (c) filament-winding.

]

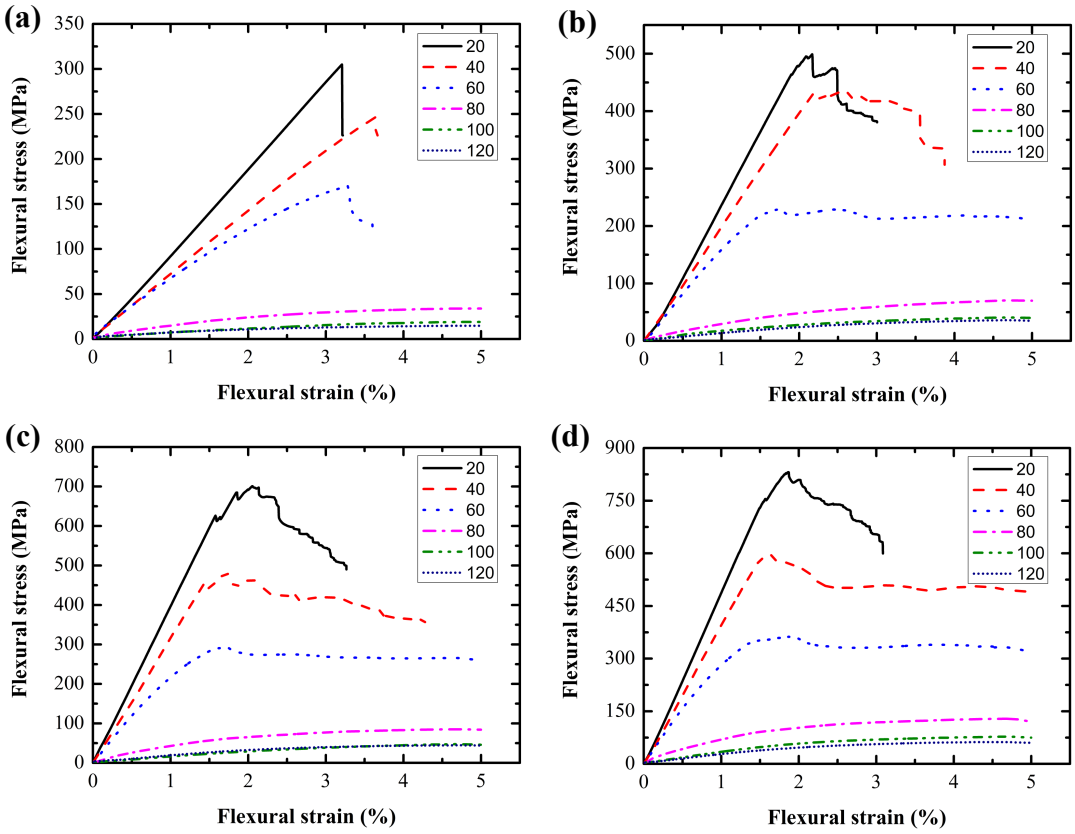

Fig. 4. Flexural stress versus strain curves at different temperatures of unidirectional carbon fiber reinforced SMP composites, (a) 16 wt.%, (b) 23 wt.%, (c) 30 wt.%, (d) 37 wt.%.

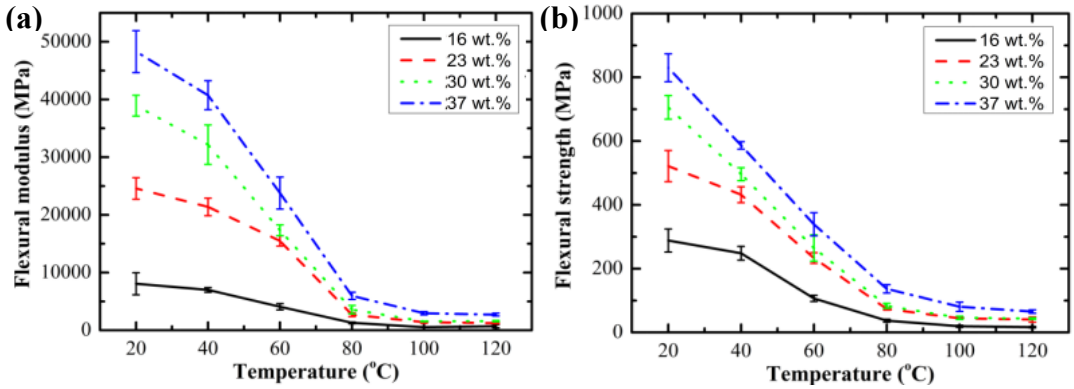

Fig. 5. Mechanical properties at different temperatures for the unidirectional carbon fiber reinforced SMP composites at different fiber mass fractions (a) flexural modulus, (b) flexural strength.

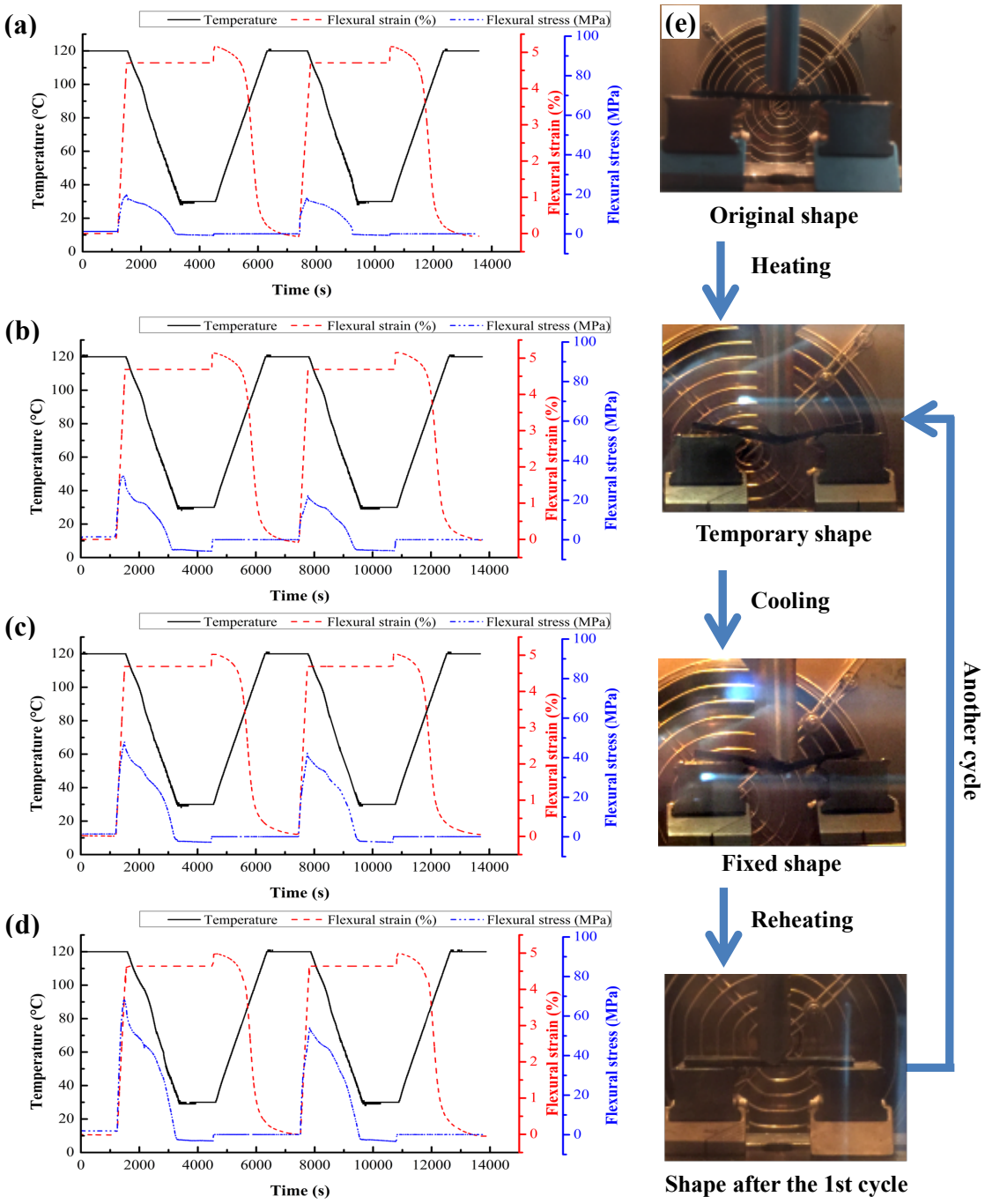

Fig. 6. Free recovery experiment curves of unidirectional carbon fiber reinforced SMP composites, (a) 16 wt.%, (b) 23 wt.%, (c) 30 wt.%, (d) 37 wt.%, (e) images at different steps.

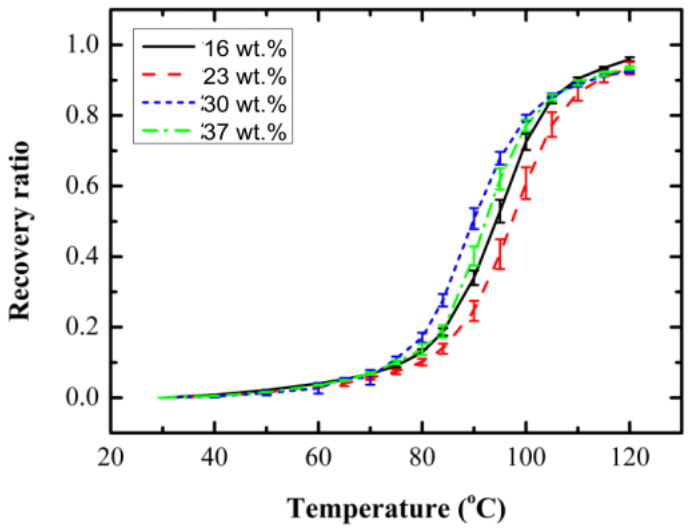

Fig. 7. Free recovery ratio-temperature curves of four types of SMP composites in the first free recovery cycle.

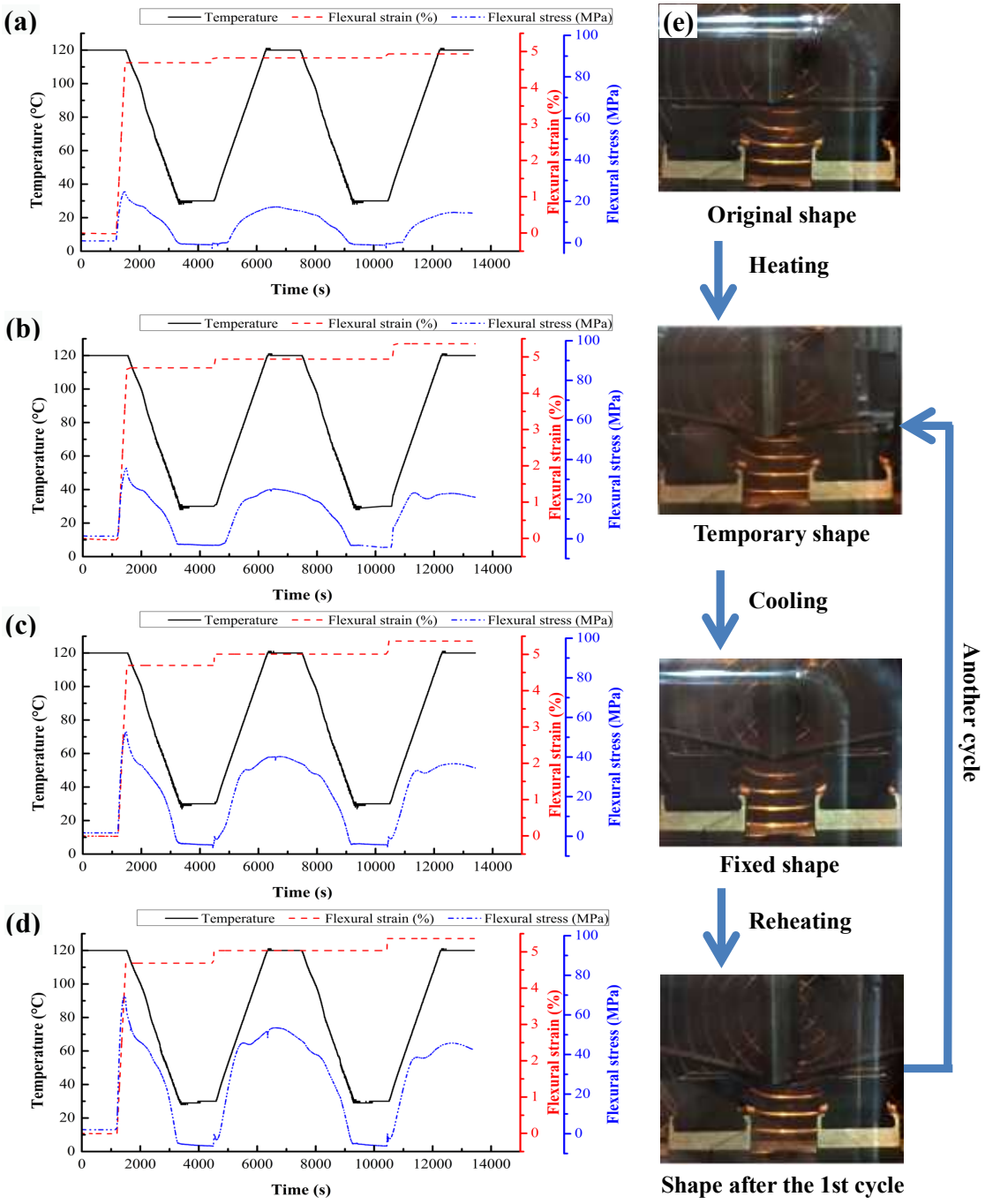

Fig. 8. Constrained displacement recovery experiment curves of unidirectional carbon fiber reinforced SMP composites, (a) 16 wt.%, (b) 23 wt.%, (c) 30 wt.%, (d) 37 wt.%, (e) images at different steps.

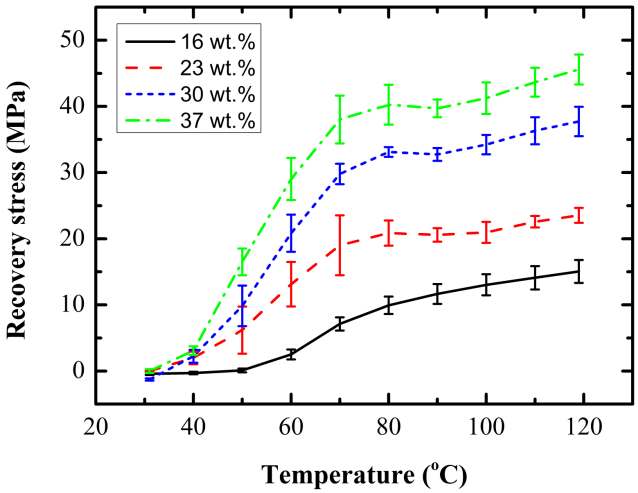

Fig. 9. Recovery stress-temperature curves of four types of SMP composites in the first constrained displacement recovery cycle

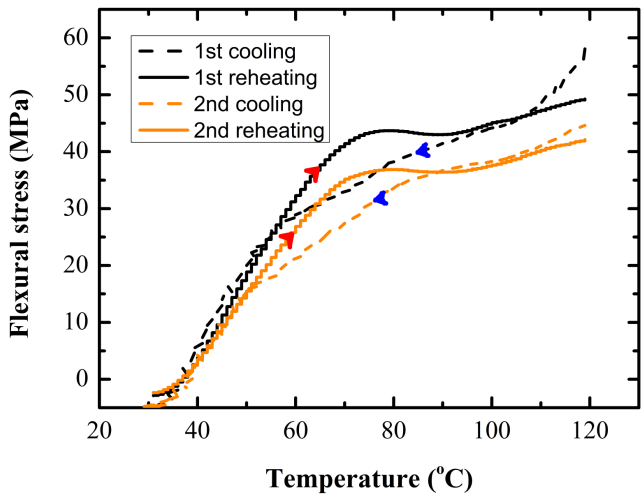

Fig. 10. Flexural stress-temperature curves for UD carbon fiber reinforced SMP composite with fiber mass fraction of 37% (the red arrow indicates reheating, the blue arrow is for cooling)

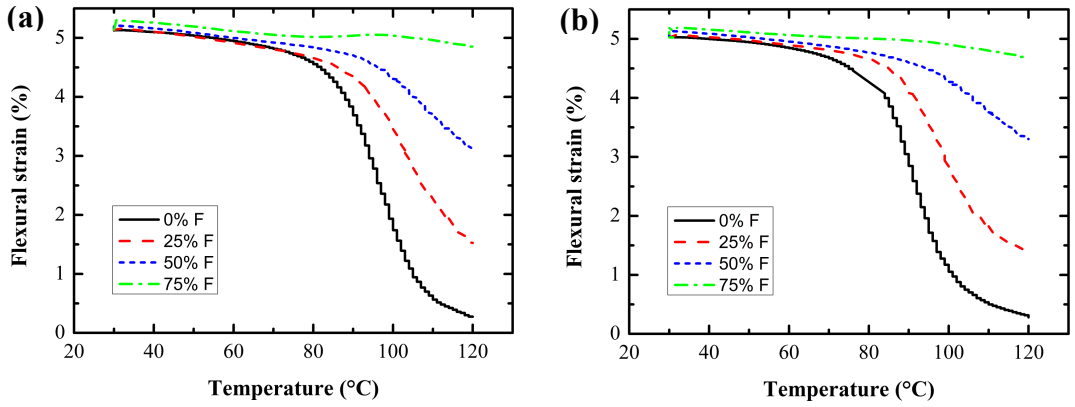

Fig. 11. Flexural strain-temperature curves during partial load recovery for the SMP composites with fiber mass fraction of (a) 23 %, (b) 37 %.

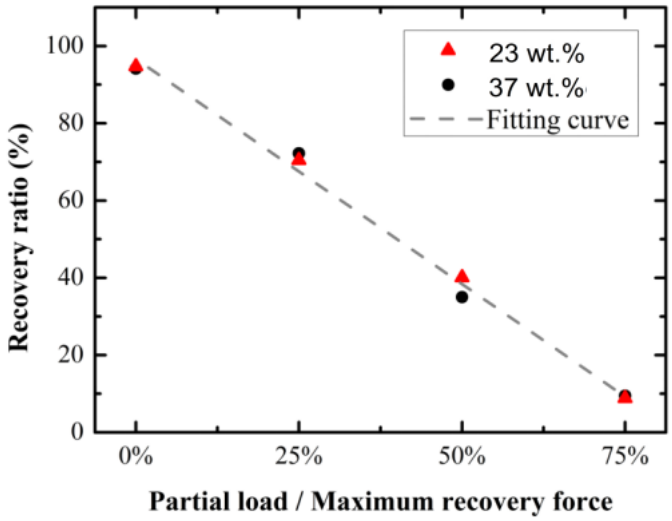

Fig. 12. Recovery ratio of SMP composites with fiber mass fraction 23% and 37% under different partial load.

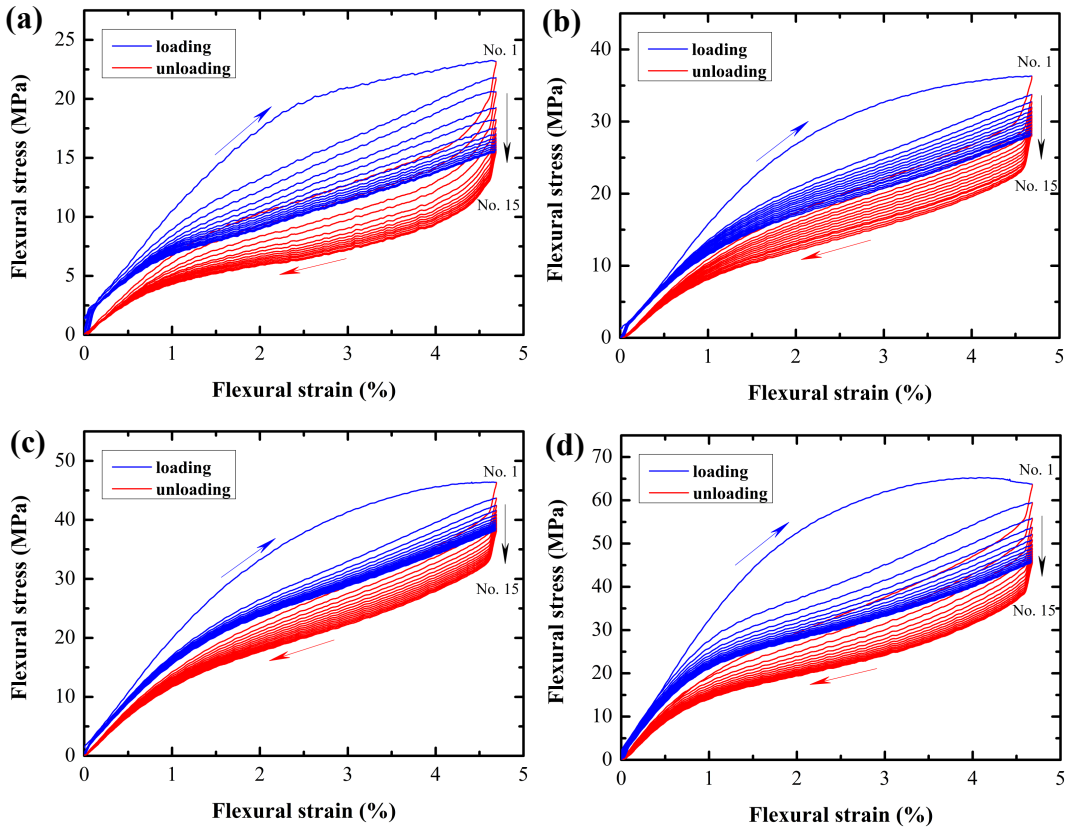

Fig. 13. Flexural stress versus strain curves of cyclic loading and unloading experiment of SMP composites with fiber mass fraction of (a) 16 %, (b) 23 %, (c) 30 %, (d) 37 % (the blue arrow indicates loading direction, the red arrow is for unloading direction, the black arrow represents the movement of the maximum load from cycle No. 1 to No. 15).

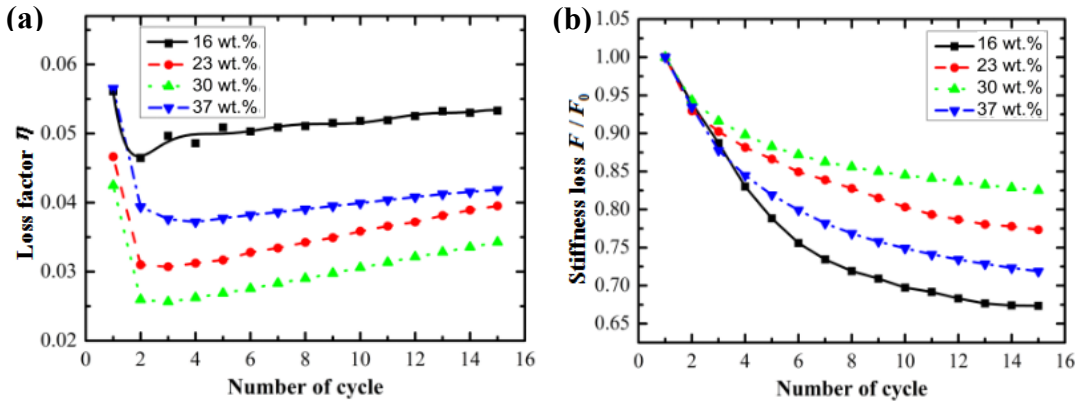

Fig. 14. Statistic of unidirectional carbon fiber reinforced SMP composites, (a) loss factor, (b) stiffness loss.

Table 1. The maximum flexural stress and additional strain during the two cycles of free recovery experiments.

fiber mass fraction of SMP composite	Maximum flexural stress during the deformation process (MPa)		Additional strain before the reheating process (%)	
	1st	2nd	1st	2nd
16 wt.%	23.0 ± 4.6	17.2 ± 2.4	0.303 ± 0.174	0.309 ± 0.172
23 wt.%	34.1 ± 2.2	24.3 ± 2.2	0.348 ± 0.092	0.345 ± 0.099
30 wt.%	50.4 ± 4.1	41.3 ± 3.1	0.351 ± 0.033	0.354 ± 0.029
37 wt.%	66.3 ± 3.2	52.8 ± 3.0	0.353 ± 0.024	0.346 ± 0.027

Table 2. The maximum recovery stress and the additional strain during the two cycles of constrained displacement recovery.

fiber mass fraction of SMP composite	Maximum recovery stress during the deformation process (MPa)		Additional strain before the reheating process (%)	
	1st	2nd	1st	2nd
16 wt.%	15.8 ± 1.6	14.7 ± 1.9	0.287 ± 0.161	0.287 ± 0.157
23 wt.%	23.9 ± 1.1	23.7 ± 1.2	0.334 ± 0.106	0.338 ± 0.087
30 wt.%	38.6 ± 2.4	37.7 ± 1.7	0.328 ± 0.042	0.342 ± 0.021
37 wt.%	47.3 ± 3.0	45.9 ± 2.3	0.323 ± 0.042	0.334 ± 0.023